

Comparison of model land skin temperature with remotely sensed estimates and assessment of surface-atmosphere coupling

I.F. Trigo^{1,2}, S. Boussetta³, P. Viterbo^{1,2},
G. Balsamo³, A. Beljaars³, I. Sandu³

Research Department

¹Instituto Português do Mar e da Atmosfera, 1749-077 Lisboa, Portugal

²Instituto Dom Luiz (IDL), 1749-016 Lisboa, Portugal

³ECMWF, Reading, UK

December 2015

Accepted for publication in the AGU Journal of Geophysical Research - Atmospheres

This paper has not been published and should be regarded as an Internal Report from ECMWF.
Permission to quote from it should be obtained from the ECMWF.



European Centre for Medium-Range Weather Forecasts
Europäisches Zentrum für mittelfristige Wettervorhersage
Centre européen pour les prévisions météorologiques à moyen

Series: ECMWF Technical Memoranda

A full list of ECMWF Publications can be found on our web site under:

<http://www.ecmwf.int/en/research/publications>

Contact: library@ecmwf.int

© Copyright 2015

European Centre for Medium Range Weather Forecasts
Shinfield Park, Reading, Berkshire RG2 9AX, England

Literary and scientific copyrights belong to ECMWF and are reserved in all countries. This publication is not to be reprinted or translated in whole or in part without the written permission of the Director. Appropriate non-commercial use will normally be granted under the condition that reference is made to ECMWF.

The information within this publication is given in good faith and considered to be true, but ECMWF accepts no liability for error, omission and for loss or damage arising from its use.

Abstract

The coupling between land surface and the atmosphere is a key feature in Earth System Modelling for exploiting the predictability of slowly evolving geophysical variables (e.g., soil moisture or vegetation state), and for correctly representing rapid variations within the diurnal cycle, particularly relevant in data assimilation applications. In this study, Land Surface Temperature (LST) estimated from Meteosat Second Generation (MSG) is used to assess the European Centre for Medium-range Weather Forecasts (ECMWF) skin temperature, which can be interpreted as a radiative temperature of the model surface. It is shown that the ECMWF model tends to slightly overestimate skin temperature during night-time and underestimate daytime values. Such underestimation of daily amplitudes is particularly pronounced in (semi-)arid regions, suggesting a misrepresentation of surface energy fluxes in those areas.

The LST estimated from MSG is used to evaluate the impact of changes in some of the ECMWF model surface parameters. The introduction of more realistic model vegetation is shown to have a positive, but limited impact on skin temperature: long integration leads to an equilibrium state where changes in the latent heat flux and soil moisture availability compensate each other. Revised surface roughness lengths for heat and momentum, however, lead to overall positive impact on daytime skin temperature, mostly due to a reduction of sensible heat flux. This is particularly relevant in non-vegetated areas, unaffected by model vegetation. The reduction of skin conductivity, a parameter which controls the heat transfer to ground by diffusion, is shown to further improve the model skin temperature.

1 Introduction

The use of remote sensing observations in numerical weather prediction (NWP) models and data assimilation systems has greatly increased in the last two decades [e.g., Bauer et al., 2010; Zheng et al., 2012]. More recently remote sensing observations have also been used for assessing model parameters that are difficult to measure or that are largely based on inference, scale-analysis or tuning, such as surface roughness length [e.g. Prigent et al., 2012], hydrological parameters [e.g. Livneh and Lettenmaier, 2012], or soil moisture [e.g. DeRosnay et al. 2013]. Land surface schemes in combination with satellite information are becoming widely used to obtain products such as evapotranspiration (e.g. see the LandFLUX-Eval initiative for a comparison of several products, Mueller et al., 2013).

Models' land surface temperature (LST) can deviate substantially from remote sensing based measurements [Garrand, 2003; Mitchell et al., 2004; Bosilovich et al., 2007; Edwards, 2010; Zheng et al., 2012; Scarino et al., 2013; Wang et al., 2014]. These errors are often associated with simplistic model representations of this geophysical variable, combined with a relatively poor knowledge of land surface parameters, such as emissivity, vegetation characteristics, roughness lengths, and coupling strength between the radiatively active surface and the underlying soil. As a consequence a high number of satellite observations are rejected for data assimilation, particularly from surface or near surface sensitive channels [e.g., English, 2008; Bauer et al., 2010; Guedj et al., 2011; Zheng et al., 2012]. The reduction of biases in modeled LST, and therefore in simulated brightness temperatures for infrared and

micro-wave sensors in window channels, constitutes one of the main motivations to improve skin temperature representation. This variable also plays a role in the partitioning between latent and sensible heat fluxes at surface; the day-to-day variability of its diurnal range in semi-arid regions is strongly correlated with soil moisture. The diurnal cycle of the land surface temperature is also controlled by the degree of coupling between the land and the atmosphere that is shown to vary greatly across models [e.g. Koster et al., 2004, 2006] and has been the subject of recent diagnostic studies to assess the coupling of land-atmosphere processes [Santanello et al., 2012] and its evolution under climatic trends [Dirmeyer et al., 2012]. It also has been the subject of field experiments like The African Multidisciplinary Monsoon Analysis (AMMA), where atmospheric and land surface observations were made to document the interactions. Boone et al. (2009) show that the precipitation errors in coupled systems like re-analyses can be very large, but also that the differences between land surface models are substantial. Although land/atmosphere coupling strengths are still rather uncertain and models have large differences, insight in the mechanisms has improved (e.g. Taylor et al., 2011, 2012; Guillod et al., 2015). Model deficiencies in LST often provide an indication of problems in surface energy fluxes and soil moisture that can affect the actual predictability of Numerical Weather Prediction (NWP) and Earth System Models (ESM) at medium and monthly-range.

In this study we present an application of LST data produced by the EUMETSAT (European organization for the Exploitation of Meteorological Satellites) Satellite Application Facility on Land Surface Analysis (LSA-SAF) [Trigo et al., 2011] from geostationary observations. This product is used to evaluate the skin temperature as simulated by the surface scheme operationally used at the European Centre for Medium-range Weather Forecasts (ECMWF). This variable corresponds to the temperature at the interface between the soil and the atmosphere. In the ECMWF Integrated Forecasting System (IFS), this interface, represented by the Hydrology Tiled ECMWF Scheme for Surface Exchanges over Land (HTESSEL) [Balsamo et al., 2009], has no heat storage. It represents the vegetation canopy for the vegetated tiles and the surface skin of soil and snow for bare soil and exposed snow tiles respectively. Thus the skin temperature of the model surface is very close to infrared-based estimations of land surface temperature from remote sensing observations.

Furthermore, we look into the impact of model parameters and representation of vegetation on the modelled skin temperature. Parameters in land surface models, such as roughness lengths for momentum/heat and the thermal coupling coefficients between skin layer and underlying soil (skin layer conductivity) are difficult to determine, despite their strong impact on surface energy fluxes and skin temperature. This work also aims to provide insight in the potential use of LST to constrain those parameters.

The impact of vegetation representation in models was analysed by Boussetta et al. [2012] for ECMWF screen variables, showing an overall improvement of near surface weather parameters when a realistic seasonal cycle leaf area index (LAI) is introduced. Other authors indicated a significant signature of vegetation seasonal and inter-annual variability on model evaporation and precipitation over land [Guillevic et al., 2002; van den Hurk et al., 2003; Lawrence and Slingo, 2004]. Vegetation state, often represented in models by LAI, is one of the main factors conditioning the partitioning between sensible and latent heat fluxes, and therefore affecting the model skin temperature. In sparsely vegetated areas, heat fluxes are essentially controlled by aerodynamic resistance, which in turn determine the evolution of skin temperature [e.g., Betts and Beljaars, 1993; Zeng and Wang, 2007; Zheng et al., 2012]. In this article we use the satellite retrievals to analyse the complementary impacts of changes in model vegetation, surface roughness, and skin layer conductivity on the modeled skin temperature and surface heat fluxes. The vegetation and surface roughness changes have already become part of the operational system at ECMWF, although the modified skin layer conductivity has not.

LST remote sensing estimations generally correspond to the radiometric temperature of the surface measured within the sensor direction, i.e., the temperature derived from a radiative energy balance of the surface, as defined by Norman and Becker [1995] and Mildrexler et al. [2011]. LST is routinely estimated from a wide range of sensors. Most remote sensing LST products make use of measurements within the atmospheric window in the thermal infra-red provided by sensors on board polar-orbiters or geostationary satellites. Changes in model soil moisture and/or surface energy fluxes often translate into changes in the daily amplitude of the model skin temperature. LST from geostationary platforms, with temporal samplings ranging from 15-minutes to hourly, are particularly well-suited to detect such signals. Currently, the LSA SAF provides 15-minute LST for clear sky conditions from the Spinning Enhanced Visible and Infrared Imager (SEVIRI) on board Meteosat Second Generation (MSG). SEVIRI LST is compared with ECMWF skin temperature to assess model runs with different land surface configurations.

The article is organized as follows. The next section presents the description of the SEVIRI/MSG data used for LST estimations, section 3 describes the skin temperature (T_{skin}) in ECMWF land surface scheme and provides a brief overview of model biases. The model experiments to assess the impact of LAI, roughness lengths and skin conductivity on T_{skin} are described in section 4. In section 5 the SEVIRI LST dataset is used to evaluate the output of the different model configurations, and the benefit of recent years' changes implemented within the ECMWF model related to vegetation and surface roughness lengths. Also the sensitivity to skin layer conductivity is discussed in this section. Finally, a discussion of the results is presented in section 6 together with a summary of the main conclusions.

2 SEVIRI/MSG Land Surface Temperature

LST derived from SEVIRI/MSG is used here to assess ECMWF modelled skin temperature. The Land Satellite Applications Facility [Trigo et al., 2011] produces an LST product every 15 minutes in near real time, covering the MSG disk centred at 0° longitude and with a spatial resolution of about 3 km at the sub-satellite point (freely available both in near real time and off-line; further information at <http://landsaf.ipma.pt>). LST is obtained by correcting top-of-atmosphere (TOA) radiances for surface emissivity, atmospheric attenuation along the path and reflection of downward radiation. The LST algorithm follows closely the generalized split window proposed by Wan and Dozier [1996] for the Advanced Very High Resolution Radiometer (AVHRR) and Moderate Resolution Imaging Spectroradiometer (MODIS), but adapted to SEVIRI response functions [Trigo et al., 2008a; Freitas et al., 2010]. The algorithm coefficients were calibrated to classes of viewing angles and total column water vapour. The split-window algorithm requires values of channel emissivity at the surface, which are estimated as a weighted average of that of bare ground and vegetation elements within each pixel [Peres and DaCamara, 2005; Trigo et al., 2008b]. The fraction of vegetation cover, also generated on a daily basis from SEVIRI/MSG data by LSA SAF [e.g., Trigo et al., 2011; Verger et al., 2009] is used as weight factor. This method produces emissivity values that are generally in line with those retrieved independently for other sensors. Differences vary with land cover type, but they are within 0.01 in the split-window bands for most surfaces [Borbas et al., 2007].

The uncertainty of LST values is also estimated taking into account the retrieval conditions in terms of atmospheric water content and viewing geometry and input uncertainties, including sensor noise, errors in the estimation of surface emissivity and in atmospheric total water vapour obtained from ECMWF forecasts [Freitas et al., 2010]. As in all remotely sensed LST products, the misclassification of pixels as clear sky may introduce large errors. The probability of cloud detection is above 96% (NWC SAF, 2012) and cloud contaminated values often appear as outliers. For most regions within the MSG disk the uncertainty of LST estimations is below 2K and pixels with estimated uncertainties higher than 4K, generally near the edge of the MSG disk, are masked out [Freitas et al., 2010].

Validation of SEVIRI LST relies on comparisons with other satellite products (e.g., MODIS) and with in-situ measurements. The latter generally reveal root mean differences (RMSD) between 1K and 2.5 K [Trigo et al., 2008a; Freitas et al., 2010; Ermida et al., 2014], depending on the surface. Given the high spatial variability of LST, better agreement is generally found for sites located in homogeneous surfaces and during night-time observations [Trigo et al., 2008a; Goettsche et al., 2013; Ermida et al., 2014; Wang et al., 2014]. The LST SEVIRI estimates used here have been shown to perform particularly well over the desert ground station maintained by the Karlsruhe Institute of Technology (KIT) in Gobabeb,

Namibia. This station is located within a fairly homogeneous landscape [Goettsche et al., 2013], where dry atmospheric conditions prevail through most of the year. Average monthly differences between satellite retrievals and in situ observations are generally within $\pm 0.5\text{K}$ and reach 1K in the rare wet months [Freitas et al., 2010]. The standard deviation of differences ranges between 1 and 2 K [Freitas et al., 2010], a value that was shown to be close to the LST spatial variability around the station by the detailed measurements carried by Goettsche et al. [2013].

3 ECMWF Model Skin Temperature

Within HTESSEL, each grid-box is split into fractions of a set of possible surface types, or tiles, namely: bare ground, low and high vegetation, intercepted water, shaded and exposed snow over land; and open and frozen water, for sea and inland water surfaces [e.g. Viterbo and Beljaars, 1995; Balsamo et al., 2009]. The skin layer is defined as the layer that intercepts and emits radiation. It represents the canopy layer for the vegetated tiles, the skin of the soil for the bare soil tile and the skin of the snow layer for the exposed snow tile. The skin layer is thermally coupled to the underlying surface through a “skin layer conductivity”, which is an empirical parameter for high / low vegetation and the conductivity of the top half of the soil and snow layers for the bare soil and exposed snow tiles respectively. The skin layer is coupled to the lowest level of the atmospheric model through standard Monin Obukov similarity based transfer laws for heat and moisture (Beljaars and Viterbo, 1998).

The energy balance equation is solved for the skin temperature (T_{skin}) of each tile, assuming that the skin layer has no heat capacity. The ECMWF skin temperature is then estimated as the weighted average of tiled T_{skin} . The energy balance assumes a single albedo for all snow-free land tiles within each model grid box, which in turn is based on snow-free monthly climatologies derived from MODIS. In the case of snow on the ground, the actual albedo will also depend on the fraction of snow cover and snow age (Dutra et al., 2010). The broad-band longwave surface emissivity is fixed constant for all tiles at 0.99.

The model skin temperature corresponds to the temperature that is obtained from thermal infra-red channels [Norman and Becker, 1995]. This means that land surface temperature products obtained from satellite measurements in the thermal infrared are particularly suited for the assessment of modelled T_{skin} over wide areas. Here we use SEVIRI LST to assess the impact of surface parameters such as the representation of vegetation, surface roughness and skin conductivity within the ECMWF model version that was operational between November 2013 and May 2015 (cycle 40r1). The model experiments and configurations are described in the next section.

4 Experiments' Configurations

A set of experiments was performed to assess the response of model skin temperature and other surface-atmosphere coupling related variables to the representation of vegetation, surface roughness parameters, and skin conductivity within the ECMWF model. The experiments consist of daily 36-hour forecasts performed with the ECMWF Integrated Forecasting System (IFS) coupled to the surface scheme HTESSEL. The forecasts experiments were run at T511 (about 40 km spatial resolution) for the months of January, April and July 2010, representative of the seasonal variability. The atmospheric fields of each forecast were initialised from the daily operational analysis at 00 UTC. Given the different time scales between land surface processes and atmosphere, and to avoid spin-up problems related to slow surface processes, the surface initial conditions of each experiment were obtained from corresponding surface offline simulations. The purpose is to have surface initial conditions (soil moisture and temperature) that are in balance with the model that is used. The offline integrations correspond to HTESSEL runs over the January 2009 – December 2010 period (i.e., at least one year before the forecast dates), using the same configuration prescribed for each forecast experiment, and driven by the ECMWF reanalysis (ERA-Interim). The different experiment setups are summarized in Table 1.

This study will be confined to forecast steps between 12 and 36 hours. This has the advantage that the forecasts are still in the deterministic range which allows a direct comparison with observations. All comparisons of model and remotely sensed LST exclude areas where the model simulates a total cloud cover higher than 10%. This threshold was selected as a compromise to ensure that T_{skin} is comparable with LST, as this is retrieved under clear sky conditions only, keeping in mind that stricter limits would decrease significantly the number of available matches. As an example, the use of a maximum model total cloud cover of 5% would lead to an overall decrease in “satellite versus model” matches of the order of 12% to 20%, depending on the month under analysis.

4.1 The Control Experiment

The configuration of the control experiment includes the prescription of a single static LAI map (Fig. 1a), and a set of roughness length values for momentum and heat (Table 2), used in the ECMWF IFS until November 2011. The values are determined by the grid box land cover type (see Table 2 and IFS documentation in <http://www.ecmwf.int/en/research/modelling-and-prediction>). The surface conductivity, Λ_{skin} , of the control is indicated in Table 3 and correspond to the set of values currently in use in the ECMWF IFS.

4.2 The Role of Vegetation

Leaf Area Index (LAI) is a dimensionless variable (m^2/m^2) defined as one half of the total leaf area per unit ground area, therefore accounting for the surface of leaves contained in a vertical column. In land surface models, LAI is often used as indicator of the vegetation state, which in turn is an essential factor controlling the partitioning between sensible and latent energy fluxes over land [e.g., Seneviratne et al., 2010].

LAI presents marked latitudinal gradients and also a strong seasonal cycle over many areas reflecting the yearly vegetation development and decay. This is captured by the monthly climatology based on MODIS [Myneni et al., 2002] shown in Figs. 1b and 1c. The comparison of MODIS LAI-based experiment and the control experiment (see Table 1) is then used to evaluate the impact of introducing a monthly-dependent LAI into the ECMWF model on skin temperature. The original MODIS-based LAI fields were adapted to fit HTESSEL, i.e., LAI were split into a low and high vegetation component, according to the respective fraction of low and high vegetation per grid-box [Boussetta et al., 2012]. Additionally, the values of minimum stomatal resistance were revised for crops (from 180 to 100 sm^{-1}), short grass (from 110 to 100 sm^{-1}) and needle-leaf trees (from 500 to 250 sm^{-1}) in an attempt to compensate for biases in two-metre humidity introduced by the LAI changes [Boussetta et al., 2012]. The LAI representation based on MODIS monthly climatology together with those changes in the minimum stomatal resistance were implemented into ECMWF operational medium-range forecast model in November 2010.

4.3 The Role of Surface Roughness

The surface roughness for heat (Z_{oH}) is a crucial parameter controlling the resistance to sensible heat transfer between the surface and the atmosphere [Beljaars and Viterbo, 1994] and values prescribed in models often lead to discrepancies between modelled T_{skin} and observations [e.g., Mitchell et al., 2004]. The roughness length for momentum (Z_{oM}) also plays a role in sensible heat fluxes, primarily because it controls the wind profile near the surface. While Z_{oM} is generally accepted to be related to the geometry of the surface elements (e.g., vegetation, buildings) within each model grid [e.g., Malhi, 1996, Zeng and Dickinson, 1998], there are several formulations proposed for Z_{oH} (or for $Z_{\text{oH}}/Z_{\text{oM}}$), involving either a constant ratio with Z_{oM} [Betts and Beljaars, 1993] or parameterizations as a function of friction velocity and fraction of vegetation cover or LAI [e.g., Raupach, 1994; Malhi, 1996; Zeng and Dickinson, 1998; Zheng et al., 2012]. Both roughness lengths vary with vegetation density, and therefore may present an annual cycle following vegetation growth and decay [e.g., Zeng and Wang, 2007; Zheng et al., 2012]. In the ECMWF model, however, both Z_{oM} and Z_{oH} assume tabulated values determined by the dominant land cover type of the model grid box (Table 2).

For a long time, ECMWF operational forecasts presented a general overestimation of 10m wind [Sandu et al., 2012]. The set of Z_{oM} values ("control" values in Table 2) was then revised in order to compensate the 10m wind biases for each surface type. The estimation of the "new values" in Table 2 assumed neutral wind profiles for all tiles [Sandu et al., 2012]. Roughness lengths for heat were also revised to balance the corresponding increase in Z_{oM} . As such, the ratio between Z_{oM} and Z_{oH} was increased from 10 to 100 for all tiles, except for forests and ice caps, where both roughness lengths are kept equal (Table 2). The new Z_{oH} table follows the trend towards higher Z_{oM} / Z_{oH} ratio suggested by previous works [e.g., Zheng et al., 2012] and was partially supported by an improvement in the simulation of SEVIRI/Meteosat brightness temperatures in the thermal window band [Sandu et al., 2012]. Here we will further assess the impact of those changes via the experiments described in Table 1 as "MODIS LAI + Z_o ", where the revised Z_{oM} and Z_{oH} values are used together with monthly maps of MODIS LAI. The revised Z_{oM} and Z_{oH} values were implemented in the ECMWF operational model in November 2011. In a next step, roughness lengths will be parameterized as a function of LAI, allowing therefore the introduction of seasonal variability in aerodynamic resistances. The full implications of such change on model simulations will be the subject of future work.

4.4 The Role of Surface Conductivity

For completeness we assess the sensitivity of model skin temperature to surface conductivity, Λ_{skin} . This parameter provides the thermal connection between the skin level and the soil (or snow deck), controlling the heat transfer to the ground by diffusion. The transfer of heat to the ground is parameterized as $[\Lambda_{\text{skin}}(T_{\text{sk}} - T_1)]$, where T_1 is the temperature of the first layer in the soil, and Λ_{skin} assumes the values indicated in Table 3. With the experiment labelled "Skin Conductivity" in Table 1, where Λ_{skin} values are halved with respect to the control, we assess the sensitivity of skin temperature to this parameter. This exercise is a first approach to test the potential use of remotely sensed LST to constrain or even estimate surface parameters, otherwise difficult to prescribe.

5 Results

Figure 2 presents the averaged difference between LSA SAF LST and ECMWF skin temperature forecasts for the three simulation months for the control run (January, April and July 2010). Both satellite and model surface temperature correspond to instantaneous fields; and the bias is shown for 0, and 12 UTC, respectively. Statistics are obtained once the LSA SAF LST data are aggregated to the model reduced gaussian grid by averaging pixels within each model grid-box. For the sake of simplicity, the upscaling procedure does not consider pixel emissivity, which is shown by Liu et al. (2006) to have a minor impact. Since LST estimations are obtained for clear sky pixels only, comparisons between model

and remote sensing estimations analysed here exclude all model grid boxes with total cloud cover higher than 10%. Grid boxes with less than 5 clear sky observations/ model simulations matches over each monthly period are masked out, leading to the inland missing data within the Meteosat shown in Fig. 2. It should be pointed out that modifications to the “5-matches” threshold do not introduce any significant changes in the main results discussed here: relaxing this value decreases the area with missing values seen in Fig. 2, but also introduces noisier patterns, particularly in regions where cloud cover is frequent; stricter thresholds further confine areas with positive/negative biases.

Skin temperature of the control run presents an overall cool bias during daytime (12 UTC panels, Fig. 2) over most of Africa and Europe and a warm bias, although generally less pronounced, during night-time (0 UTC panels, Fig. 2). This underestimation of the daily amplitude of T_{skin} seems to be particularly pronounced over semi-arid regions (North Africa, Sahara, Namibia). A different pattern is seen over subtropical regions during the wet season (see e.g., tropical Africa and the Sahel/West Africa in Figs. 2d and 2f), where the model 12UTC T_{skin} is warmer than satellite estimations. Although grid boxes with less than 5 clear sky observations were masked-out, signal contamination in areas with persistent cloud cover, such as the wet season tropics, cannot be excluded.

The warm bias over the North-western African coast in July (day and night time) is not clearly understood and its possible link with the ECMWF IFS simulation of the monsoon onset needs to be assessed over a multi-year period. It should also be mentioned that the uncertainty of LST estimations increases significantly for large viewing angles [Freitas et al., 2011]. Therefore, the large biases in areas near the edge of the Meteosat disk, such as the Arabian Peninsula (where local time differences with respect to UTC are also relevant), or Scandinavia, must be taken with caution.

A more robust assessment of T_{skin} bias would require the analysis of a longer period. However, the results presented in Figure 2 do not deviate greatly from those already discussed in Trigo and Viterbo (2003), where a first comparison between ECMWF model and Meteosat-7 and Meteosat-5 observations was carried out for the period between February and October 2001. Although the study was focused on modelled TOA brightness temperatures for the Meteosat thermal window channel, it pointed to deficiencies in the cloud screening of the satellite data, particularly in tropical regions, and systematic underestimation of the diurnal cycle of the modelled brightness temperature in clear-sky. Since that study, the cloud screening has been largely improved in SEVIRI/MSG radiances essentially due to the higher spectral and spatial resolutions.

The impacts of the different model changes on skin temperature are evaluated in terms of the difference in the mean absolute error of the control versus experiment (i.e., a positive impact corresponds to a lower absolute error in the experiment); SEVIRI LST is being used here as reference for skin temperature:

$$impact(LST) = |LST_{ctt} - LST_{SEVIRI}| - |LST_{exp} - LST_{SEVIRI}| \quad (1)$$

5.1 Evaluation of the Impact of changes in the Vegetation

The impact of introducing a MODIS-based monthly LAI climatology on the model skin temperature is shown in Fig. 3, revealing neutral impact almost everywhere. Positive impact, corresponding to a decrease in 12 UTC Tskin bias of the order of 0.5 K, is seen over limited regions: the area stretching to the south of the Sahel (January and July, in Figs 3b and 3f), South-western Europe and Middle East (Fig. 3d). The impact on night-time temperatures is even smaller.

The introduction of a more realistic representation of vegetation in the ECMWF model, and particularly the significant change in the values of LAI used in the model (see Fig. 1a versus 1b and 1c) would be expected to have a stronger impact on the surface energy budget and therefore on the modelled skin temperature. Figure 1 shows that MODIS LAI values are generally lower than those in the static map, which in turn would be expected to decrease evapotranspiration in mid-latitudes during spring/summer and in the tropics and subtropics. This effect explains the weak positive impact on daytime temperature described above. Further evidence is shown in Fig. 4, where the impact on Tskin is plotted against changes in evapotranspiration with respect to the control experiment, for two distinct regions and periods: (i) an area in the West African monsoon (WAM) region (20°W – 10°E ; 2.5°N – 17.5°N) in January and; (ii) the Iberian Peninsula (9.5°W – 0°E ; 36°N – 44°N) in April. Figure 4 also emphasizes the variability among different land cover types within each area. In the WAM region, positive impacts are identified for grid boxes dominated by interrupted forest and by tall grass, which mark the transition between savannah and semi-desert landscape. The largest values, however, occur for the evergreen broad-leaf type, dominating the landscape further south of the WAM box, and corresponding to the area with positive impact along the Gulf of Guinea shown in Fig. 3b. In the Iberian Peninsula, the rather low impact on Tskin seems nevertheless to be stronger again for interrupted forest. For both areas, the positive impact on 12 UTC Tskin corresponds to an increase of daytime skin temperature and also in its daily amplitude, due to a reduction in evapotranspiration with respect to the control. As mentioned before, the magnitude of the impact of the revised LAI on Tskin is limited, and in some cases even slightly negative, as for “crops” land cover types. The reduction in stomatal resistance for this vegetation type (Table 1), as well as for, e.g., “tall grass”, contributes to decrease the sensitivity of evapotranspiration to the change (drop) in vegetation, attenuating the impact on skin temperature.

The rather small changes seen in the diurnal amplitude of Tskin when LAI is significantly reduced in the model are likely associated to an equilibrium reached during the off-line simulations. As described in section 4, the MODIS LAI experiments start from an offline HTESSEL run over 1-year period using the same “MODIS LAI” configuration, and driven by ERA-Interim. The LAI decrease in the offline

run leads indeed to less evaporation in most places, which in turn leads to a wetter soil which would compensate for the decrease in evaporation associated with the change in LAI. When compared with the control run, soil moisture of “LAI MODIS” simulations presents significantly higher values (Fig. 5), with particularly pronounced changes to the south of the Sahel area. It is worth noting that this increase in soil moisture would be much smoother if the LAI experiment would start from the control offline run, leading to signals stronger than those shown in Fig. 3. It is shown that in the long run, changes in evapotranspiration rates and soil moisture balance each other and lead to a small impact on surface temperature.

5.2 Impact of Model Surface Roughness

Figure 6 shows the impact on model skin temperature, of the revised roughness lengths, added to the LAI modifications analysed in the previous section (“LAI + Z_o ” experiment in Table 1). As in the MODIS LAI experiment, this is negligible for night-time conditions. However, for daytime, the signal is much stronger, with an overall positive impact, particularly over arid regions. The new Z_{oM} and Z_{oH} values lead to a significant reduction of the systematic underestimation of model daily amplitudes of skin temperature when compared to the remote sensed estimations.

The overall impact on daytime LST in most regions is positive, although few areas present slight negative impact such as the Western Sahara and the Arabian Peninsula mainly in July. In these two cases the control overestimates the 12 UTC skin temperature (Fig. 2), and therefore the revised roughness length table reinforces the deviation from satellite estimates.

The increase in Z_{oM} for many biomes leads to a tighter coupling between atmosphere and surface, while the reduction of the roughness length for heat leads to an increase in the aerodynamic resistance and therefore to lower heat fluxes. Over areas dominated by “desert” or “bare ground” tiles, such as the Sahara and Arabian Peninsula, roughness lengths for momentum remain unchanged. There, the positive impact on skin temperature can only be attributed to the reduction in roughness length for heat (Table 2) and the respective increase in the resistance to heat transfer. As mentioned before, the roughness is tabulated according to the land use type, and it is currently decoupled from the vegetation state (i.e. there is no seasonal variation of the tabulated values following the vegetation cycle). The introduction of such link would most likely increase the sensitivity of the model to the vegetation state; this will be the subject for a future study.

5.3 Impact of Model Skin Conductivity

The impact of reducing the skin conductivity, Λ_{skin} , by half with respect to the control (Table 3) is shown in Fig. 7. The overall pattern does not differ much from that obtained in the previously described

experiment (see Fig 6), but with an overall strengthening of the signal, both for positive and negative impact cases. This applies also to night-time skin temperatures, which up to now had only been marginally affected by the other model changes with respect to the control. Figures 7a, 7c, and 7e indicate a decrease in the 0UTC T_{skin} bias of the order of 0.8 to 1.6 K in areas where the control overestimates skin temperature with respect to SEVIRI estimates (Figure 2a, 2c, and 2e). The impact is however, slightly negative over regions which presented negligible or slightly negative bias. The reduction of Λ_{skin} implies reducing the magnitude of ground heat flux, G . As a result, attenuated values of: (i) daytime downward ground flux lead to increased surface temperatures; (ii) night-time upward ground fluxes contribute to intensify the cooling.

6 Discussion and Conclusions

Several studies have reported pronounced cold biases in modelled surface temperatures, particularly during daytime over arid regions, when compared either to satellite retrievals or to in situ measurements [e.g, Garrand, 2003; Edwards, 2010; Zheng et al., 2012]. Biases of this type have also been previously identified in the ECMWF model [Trigo and Viterbo, 2003]. These results are also in line with the comparison of model T_{skin} and satellite estimates of LST obtained for the control experiment analysed in this study. The surface scheme used in the control simulation includes a static map of LAI and tabulated values of roughness lengths for heat and momentum operational in the ECMWF model until 2010 and 2011, respectively. The satellite LST corresponds in turn to the temperature of the surface within the sensor field-of-view.

There are many factors that can contribute to the systematic deviations of the land surface temperature with respect to remote sensing estimations reported for many models. A misrepresentation of surface energy fluxes either because of deficiencies in the parameterization of aerodynamic resistances or in the partitioning between latent and sensible heat fluxes are frequent causes of these deviations. In this study we use geostationary Land Surface Temperature (LST) estimations to analyse the impact of changes in the model vegetation and roughness lengths for momentum and heat – parameters that control energy and water exchanges between the surface and the atmosphere – and skin conductivity, which controls the ground flux. There are a myriad of other causes that lead to errors in T_{skin} , including the representation of clouds, water vapour, which strongly impact on the short-wave downward radiation at the surface. These are out of scope of this work and by restricting the analysis to model clear sky cases, their impact might be expected to be reduced, although not eliminated.

The introduction of revised LAI reproducing a realistic vegetation annual cycle at global scale has a rather limited impact on the model T_{skin} , with a slight improvement (decreases in biases are generally

within 0.5°C) with respect to satellite observations over semi-arid or sparsely vegetated regions (e.g., WAM, Iberian Peninsula). The new mostly lower LAI leads to lower evapotranspiration [e.g. Guillevic et al., 2002] and the long integration with the offline runs allows the model to reach an equilibrium state with higher soil moisture which would lead to an evaporation increase. The two effects compensate each other to attenuate the impact on T_{skin} . Figure 8a shows the sensitivity of surface latent heat (i.e., average of experiment minus control field) for July 2010. Despite the reduction in latent fluxes (LE) observed in tropical regions (including the WAM region), the mid-to-high latitudes regions showed an increase in evapotranspiration. This can be attributed to the higher soil moisture availability and to the reduction in the stomatal resistance (particularly in needle leaf forests). The signal in latent heat flux is partially compensated by an opposite behaviour in sensible heat flux (H, Fig. 8b). Previous studies indicated the relevance of model vegetation for the adequate modelling of the various components of the surface energy balance leading to improvements in screen variables [Knott et al., 2009; Boussetta et al., 2012]. A revision of the vertical soil discretisation (not shown here) is expected to improve the match to the LST, particularly over sparsely vegetated areas. Synergy of this revision with a more realistic evolution of the vegetation cover would extend the warming effects into mid-latitude areas. Preliminary tests with a 10-layer soil discretisation (recently implemented offline with 1, 2, and 4 cm top layers in place of the current 7cm layer) indicate a warming impact on T_{skin} over dryland.

The adjustment of roughness lengths for heat and momentum leads to an overall positive impact on daytime skin temperature, generally due to a reduction of sensible heat flux as a result of lower values of Z_{oH} . The positive impact is particularly relevant in non-vegetated areas that remained unaffected by the changes in the vegetation representation. In this regions, the [LAI + Z_o] experiment presents a clear decrease in the average sensible fluxes when compared with the control (see e.g., Fig. 8d), which cannot be compensated by LE (see e.g., fig. 8c).

The reduction of skin conductivity is shown to further strengthen the positive impact on model T_{skin} . It is interesting to notice, however, that this further modification in Λ_{skin} reduces the sensitivity of LE and H, when compared with the [LAI + Z_o] experiment: Figs. 8e and 8f suggest lower differences in LE and H with respect to the control, than Figs. 8c and 8d.

LST estimates from geostationary platforms allow the assessment of the model diurnal cycle under clear sky conditions. For simplicity, this work was focused on two time slots (0 and 12 UTC) representative of night-time and daytime within most of Meteosat disk (mostly Europe and Africa). Figure 9 presents daily cycles averaged over January 2010, for two model grid points over the Sahara and the WAM region, respectively, where clear sky conditions prevail in that period; the number of clear sky observations/model simulations is also given. Figure 9 stresses not only the large variability in space of

the discrepancies between model and satellite, as analysed in this study, but also their strong diurnal cycle. The figure illustrates well the impact of the experiments analysed here on model Tskin, with limited impact of the introduced model modifications over the WAM, despite the large departures with respect to SEVIRI. Other effects, such as the phase mismatch between model and satellite surface temperatures (Fig. 9b) and differences in observed and modelled cloud cover are also shown.

The year 2010 was characterized by strong warm temperature anomalies over many parts of the world [Blunden et al., 2011], including Northern Africa and Europe, which was affected by a heat wave in July [Barriopedro et al., 2011]. Similar model experiments to those analysed here run for 2008-2009, but not presented because of differences in the spatial resolution, or initialization cycles, indicated patterns and magnitudes of Tskin biases comparable to those found for the period under study. Such preliminary studies also indicated that model initialization, through off-line runs as done here or via assimilation cycles, is crucial in determining the impact of surface processes on model Tskin. Many factors controlling the model radiation and energy budget at the surface have yet to be studied. This paper showed that remotely sensed LST have the potential to evaluate model changes and may be used to optimize model surface parameters that are non-observable or otherwise difficult to determine, such as skin conductivity or roughness lengths. Parameter adjustment would, however, require a thorough analyses of all components of the surface energy budget and their implications to many other model variables.

Acknowledgements

This work was carried out within the context of the LSA SAF project (<http://landsaf.ipma.pt>) funded by EUMETSAT. The SEVIRI/MSG Land Surface Temperature used here are freely available from <http://landsaf.ipma.pt>. Information on ECMWF model and data is provided at <http://www.ecmwf.int>.

References

- Balsamo, G., P. Viterbo, A. Beljaars, B. Van den Hurk, A.K. Betts and K. Scipal (2009), A revised hydrology for the ECMWF model: Verification from field site to terrestrial water storage and impact in the Integrated Forecast System. *J. Hydrometeorol.*, **10**, 623–643, doi:10.1175/2008JHM1068.1171.
- Bauer P, A.J. Geer, P. Lopezand D. Salmond (2010), Direct 4D-Var assimilation of all-sky radiances. Part I: Implementation. *Q. J. R. Meteor. Soc.* **136**, 1868–1885, DOI:10.1002/qj.659.
- Barriopedro D., Fisher E., Luterbacher J., Trigo R.M., García-Herrera R., (2011), The hot summer of 2010: redrawing the temperature record map of Europe. *Science*, **322**, 220. DOI: 10.1126/science.1201224

Beljaars, A.C.M and P. Viterbo (1994), The sensitivity of winter evaporation to the formulation of aerodynamic resistance in ECMWF model. *Bound.-Layer Meteor.*, **71**, 135-149.

Beljaars, A. and P. Viterbo (1998), The role of the boundary layer in a numerical weather prediction model, in: *Clear and cloudy boundary layers*, A.A.M. Holtslag and P. Duynkerke (eds.), Royal Netherlands Academy of Arts and Sciences, p. 287-304, Amsterdam, North Holland Publishers.

Betts, A.K. and A.C.M. Beljaars (1993), Estimation of effective roughness length for heat and momentum from FIFE data. *Atmos. Res.*, **30**, 251-261.

Blunden, J., D. S. Arndt, and M. O. Baringer, 2011: State of the Climate in 2010. *Bull. Amer. Meteor. Soc.*, **92**, S1–S236. DOI: 10.1175/1520-0477-92.6.S1

Boone, A., B. Decharme, F. Guichard, P. de Rosnay, G. Balsamo, A. Beljaars, F. Chopin et al. (2009), The AMMA land surface model intercomparison project (ALMIP). *Bull. Amer. Meteor. Soc.*, **90**, 1865-1880.

Borbas, E.E., L. Moy, S.W. Seemann, R.O. Knuteson, P. Antonelli, J. Li, H.-L. Huang, I. Trigo and L. Zhou (2007), A Global infrared Land Surface Emissivity Database and its validation. *Symposium on Integrated Observing and Assimilation Systems for Atmosphere, Oceans, and Land Surface*, 11th, San Antonio, TX, 14-18 January 2007. American Meteorological Society, Boston, MA, 2007, Paper P2.7

Bosilovich, M.G., J.D. Radakovich, A. da Silva, R. Todling and F. Verter (2007), Skin temperature analysis and bias correction in a coupled land-atmosphere data assimilation system. *J. Meteor. Soc. Jap.*, **85A**, 205-228.

Boussetta, S., G. Balsamo, A. Beljaars, T. Kral and L. Jarlan (2012), Impact of a satellite-derived Leaf Area Index monthly climatology in a global Numerical Weather Prediction model. *Int. J. Remote Sensing.*, **34**, 3520-3542, doi:10.1080/01431161.2012.716543.

Chen, Y., K. Yang, D. Zhou, J. Qin, and X. Guo (2010), Improving the Noah Land Surface Model in Arid Regions with an Appropriate Parameterization of the Thermal Roughness Length. *J. Hydrometeor*, **11**, 995–1006, doi: <http://dx.doi.org/10.1175/2010JHM1185.1>.

de Rosnay, P., M. Drusch, D. Vasiljevic, G. Balsamo, C. Albergel and L. Isaksen (2013), A simplified Extended Kalman Filter for the global operational soil moisture analysis at ECMWF. *Q. J. R. Meteor. Soc.*, **139**, 1199-1213.

Dirmeyer, P.A., B.A. Cash, J.L. Kinter III, T. Jung, L. Marx, C. Stan, P. Towers, N. Wedi, J.M. Adams, E.L. Altshuler, B. Huang, E.K. Jin and J. Manganello (2012), Evidence for enhanced land-atmosphere feedback in a warming climate. *J. Hydrometeor.*, **13**, 981-995, doi: 10.1175/JHMD-11-0104.1.

Dutra, E., G. Balsamo, P. Viterbo, P. Miranda, A. Beljaars, C. Schar and K. Elder (2010), An improved snow scheme for the ECMWF land surface model: Description and offline validation. *J. Hydrometeor.* **11**, 7499-7506.

Edwards J.M. (2010), Assessment of Met Office forecasting models with SEVIRI LSTs. *Proceedings of the 4th LSA SAF User Training Workshop*, 15 – 17 November 2010, Météo-France, Toulouse, France.

English, S.J. (2008), The importance of accurate skin temperature in assimilation radiances from satellite sounding instruments. *IEEE Trans. Geosc. Sens.*, **46**, 403-408, doi:10.1109/TGRS.2007.902413.

Ermida, S.L., I.F. Trigo, C.C. DaCamara, F.M. Götsche, F.S. Olesen and G. Hulley (2014), Validation of remotely sensed surface temperature over an oakwood landscape - The problem of viewing and illumination geometries. *Remote Sens. Env.*, **148**, 16-27, doi: dx.doi.org/10.1016/j.rse.2014.03.016.

Freitas, S.C., I.F. Trigo, J.M. Bioucas-Dias and F.-M. Goettsche (2010), Quantifying the Uncertainty of Land Surface Temperature Retrievals From SEVIRI/Meteosat. *IEEE Trans. Geosci. Remote Sens.*, DOI: 10.1109/TGRS.2009.2027697.

Garand, L. (2003), Toward an Integrated Land–Ocean Surface Skin Temperature Analysis from the Variational Assimilation of Infrared Radiances. *J. Appl. Meteor.*, **42**, 570–583, doi: 10.1175/1520-0450(2003)042<0570:TAILSS>2.0.CO;2,

Goettsche, F.M., F.S. Olesen and A. Bork-Unkelbach (2013): Validation of land surface temperature derived from MSG/SEVIRI with in situ measurements at Gobabeb, Namibia. *Int. J. Remote Sens.*, **34**, 3069-3083. doi: 10.1080/01431161.2012.716539.

Guedj, S., F. Karbou and F. Rabier (2011), Land surface temperature estimation to improve the assimilation of SEVIRI radiances over land. *J. Geophys. Res.*, **116**, D14107, doi:10.1029/2011JD015776.

Guillevic, P., R.D. Koster, M.J. Suarez, L. Bounoua, G J. Collatz, S. O. Los and S.P.P. Mahanama (2002), Influence of the interannual variability of vegetation on the surface energy balance – a global sensitivity study. *J. Hydrometeor.*, **3**, 617-629.

Guillod, B.P., B. Orlowsky, D.G. Miralles, A.J. Teuling and S.I. Seneviratne (2015), Reconciling spatial and temporal soil moisture effects on afternoon rainfall, *Nature Communications*, **6**, 6443.

Kabsch, E., F.S. Olesen, and A. J. Prata (2008), Initial results of the land surface temperature (LST) validation with the Évora, Portugal ground-truth station measurements. *Int. J. Remote Sensing*, **29**, 5329-5345.

Knote, C., G. Bonafe and F. Di Giuseppe (2009), Leaf Area Index Specification for Use in Mesoscale Weather Prediction Systems. *Mon. Wea. Rev.*, **137**, 3535-3550.

Koster R.D., P.A. Dirmeyer, Z. Guo, G. Bonan, E. Chan, P. Cox, C.T. Gordon, S. Kanae, E. Kowalczyk, D. Lawrence, P. Liu, C.H. Lu, S. Malyshev, B. McAvaney, K. Mitchell, D. Mocko, T. Oki, K. Oleson, A. Pitman, Y.C. Sud, C.M. Taylor, D. Verseghy, R. Vasic Y. Xue, T. Yamada and GLACE Team (2004), Regions of strong coupling between soil moisture and precipitation. *Science*, **305** 1138-40.

Koster, R.D. and Coauthors (2006) GLACE: The Global Land–Atmosphere Coupling Experiment. Part I: Overview. *J. Hydrometeor*, **7**, 590–610, doi: <http://dx.doi.org/10.1175/JHM510.1>.

Lawrence D.M. and J.M. Slingo (2004), An annual cycle of vegetation in a GCM. Part I: implementation and impact on evaporation, *Clim. Dyn.*, **22**, 87-105

Liu, Y., T. Hiyama and Y. Yamaguchi (2006), Scaling of land surface temperature using satellite data: A case examination on ASTER and MODIS products over a heterogeneous terrain area. *Remote Sens. Env.*, **105**, 115-128, doi:10.1016/j.rse.2006.06.012.

Livneh, B. and D.P. Lettenmaier, (2012), Multi-criteria parameter estimation for the Unified Land Model. *Hydrol. Earth Syst. Sci.*, **16**, 3029-3048. doi:10.5194/hess-16-3029-2012.

Malhi, Y. (1996), The behaviour of the roughness length for temperature over heterogeneous surfaces. *Q. J. R. Meteor. Soc.*, **122**, 1095-1125.

Mildrexler, D.J., M. Zhao, and S.W. Running (2011), Satellite Finds Highest Land Skin Temperatures on Earth. *Bull Americ. Met. Soc.*, DOI:10.1175/2011BAMS3067.1

Mitchell, K. and Coauthors (2004), The multi-institution North American Land Data Assimilation System (NLDAS): Utilizing multiple GCIP products and partners in a continental distributed hydrological modeling system. *J. Geophys. Res.*, **109**, D07S90, doi:10.1029/2003JD003823.

Mueller, B., M. Hirschi, C. Jimenez, P. Ciais, P.A. Dirmeyer, A.J. Dolman, J.B. Fisher, M. Jung, F. Ludwig, F. Maignan, D. Miralles, M.F. McCabe, M. Reichstein, J. Sheffield, K.C. Wang, E.F. Wood, Y. Zhang and S.I. Seneviratne (2013), Benchmark products for land evapotranspiration: LandFlux-EVAL multi-dataset synthesis. *Hydrol. Earth Syst. Sci.*, **17**, 3707-3720, doi:10.5194/hess-17-3707-2013.

Myneni, R. B. et al. (2002), Global products of vegetation leaf area and fraction absorbed PAR from year one of MODIS data. *Remote Sens. Env.*, **83**, 214-231.

Norman, J.M. and F. Becker (1995), Terminology in thermal infrared remote sensing of natural surfaces. *Agric. For Met.*, **77**, 153-166.

NWC SAF (2012): Validation Report for “Cloud Products” (CMa-PGE01 v3.2, CT-PGE02 v2.2 & CTTH-PGE03 v2.2), SAF/NWC/CDOP/MFL/SCI/VR/06, Issue 1, Rev.0, 15 February 2012, 31 pp. (<http://www.nwcsaf.org>).

Peres, L.F. and C.C. DaCamara (2005), Emissivity Maps to Retrieve Land-Surface Temperature from MSG/SEVIRI, *IEEE Trans. Geosci. Remote Sens.*, **43**, 1834-1844.

Prigent, C., C. Jimenez and J. Catherinot (2012), Comparison of satellite microwave backscattering (ASCAT) and visible/near-infrared reflectances (PARASOL) for the estimation of aeolian aerodynamic roughness length in arid and semi-arid regions. *Atmos. Meas. Tech.*, **5**, 2703-2712, doi:10.5194/amt-5-2703-2012.

Raupach, M.R. (1994), Simplified expressions for vegetation roughness length and zero-plane displacement as a function of canopy height and area index. *Bound.-Layer Meteor.*, **71**, 211–216.

Sandu, I., A. Beljaars, G. Balsamo and A. Ghelli (2012), Revision of the surface roughness length table. *ECMWF Newsletter* No. 130 – Winter 2011/2012, pp 8-10.

Santanello, J., C. Peters-Lidard, A. Kennedy and S. Kumar (2012), Diagnosing the Nature of Land-Atmosphere Coupling: A Case Study of Dry/Wet Extremes in the U. S. Southern Great Plains. *J. Hydrometeor.*, **14**, 3-24.

Scarino B., P. Minnis, R. Palikonda, R.H. Reichle, D. Morstad, C. Yost, B. Shan and Q. Liu (2013) Retrieving Clear-Sky Surface Skin Temperature for Numerical Weather Prediction Applications from Geostationary Satellite Data. *Remote Sens.*, **5**, 342-366, DOI:10.3390/rs5010342.

Seneviratne, S.I., T. Corti, E.L. Davin, M. Hirschi, E.B. Jaeger, I. Lehner, B. Orlowsky and A.J. Teuling, 2010: Investigating soil moisture-climate interactions in a changing climate: A review. *Earth-Science Reviews*, **99**, 125-161, doi:10.1016/j.earscirev.2010.02.004.

Taylor, C.M., A. Gounou, F. Guichard, P.P. Harris, R.J. Ellis, F. Couvreux and M. De Kauwe (2011), Frequency of Sahelian storm initiation enhanced over mesoscale soil-moisture patterns, *Nature Geoscience*, **4**, 430-433.

Taylor, C.M., R.A.M. de Jeu, F. Guichard, P.P. Harris and W.A. Dorigo (2012), Afternoon rain more likely over drier soils. *Nature*, **489**, 423-426, 10.1038/nature11377.

Trigo, I.F., C.C. DaCamara, P. Viterbo, J.-L. Roujean, F. Olesen, C. Barroso, F. Camacho-de Coca, D. Carrer, S.C. Freitas, J. García-Haro, B. Geiger, F. Gellens-Meulenberghs, N. Ghilain, J. Meliá, L. Pessanha, N. Siljamo and A. Arboleda (2011), The Satellite Application Facility on Land Surface Analysis. *Int. J. Remote Sens.*, **32**, 2725-2744, doi: 10.1080/01431161003743199.

Trigo, I.F., I.T. Monteiro, F. Olesen and E. Kabsch (2008a), An assessment of remotely sensed land surface temperature. *J. Geophys. Res.*, **113**, D17108, doi:10.1029/2008JD010035.

Trigo, I.F. and L.F. Peres, C.C. DaCamara and S.C. Freitas (2008b), Thermal Land Surface Emissivity retrieved from SEVIRI/Meteosat. *IEEE Trans. Geosci. Remote Sens.*, Doi: 10.1109/TGRS.2007.905197.

Trigo I.F. and P. Viterbo (2003), Clear sky window channel radiances: a comparison between observations and the ECMWF model. *J. App. Meteor.*, **42**, 1463-1479.

Van den Hurk, B., P. Viterbo and S. Los (2003), Impact of leaf area index seasonality on the annual land surface evaporation in a global circulation model. *J. Geophys. Res.*, **108**, D64191, doi:10.1029/2002JD002846.

Verger, A., F. Camacho, F.J. García-Haro and J. Meliá (2009), Prototyping of Land-SAF leaf area index algorithm with VEGETATION and MODIS data over Europe, *Remote Sens. Environ.*, **113**, 2285–2297, DOI:10.1016/j.rse.2009.06.009.

Viterbo, P. and A.C.M. Beljaars (1995), An improved land surface parametrization scheme in the ECMWF model and its validation. *J. Climate*, **8**, 2716-2748.

Wan, Z. and J. Dozier (1996), A generalized split-window algorithm for retrieving land surface temperature from space, *IEEE Trans. Geosci. Remote Sens.*, **34**, 892–905.

Wang, A., M. Barlage, X. Zeng and C. S. Draper (2014), Comparison of land skin temperature from a land model, remote sensing and in situ measurement. *J. Geophys. Res.*, **119**, 3093-3106, DOI: 10.1002/2013JD021026.

Zeng, X. and R.E. Dickinson (1998), Effect of surface sublayer on surface skin temperature and fluxes. *J. Clim.*, **11**, 537-550.

Zeng, X. and A. Wang (2007), Consistent parameterization of roughness length and displacement height for sparse and dense canopies in land models. *J. Hydrometeorol.*, **8**, 730-737, DOI: 10.1175/JHM607.1.

Zheng, W., H. Wei, Z. Wang, X. Zeng, J. Meng, M. Ek, K. Mitchell and J. Derber (2012), Improvement of daytime land surface skin temperature over arid regions in the NCEP GFS model and its impact on satellite data assimilation. *J. Geophys. Res.*, **117**, D06117, Doi: 10.1029/2011JD015901.

Table 1. Description of model experiments.

Experiment	Description	Initial surface conditions	Common to all experiments
Control	<ul style="list-style-type: none"> - Constant LAI. - Non-revised Z_{oM}, Z_{oH} (see Table 2). - Non-revised minimum stomatal resistance (Boussetta et al., 2012). 	<ul style="list-style-type: none"> Off-line runs driven by ERA-Interim (Jan 2009 – Dec 2010), with: - Constant LAI - Non-revised Z_{oM}, Z_{oH} (see Table 2). - Non-revised minimum stomatal resistance. 	<ul style="list-style-type: none"> - Forecast experiments run at T511 (about 40 km resolution). - Daily 36-hour forecasts start from the operational 00 UTC analyses of the atmospheric fields.
MODIS LAI	<p>As above, but with:</p> <ul style="list-style-type: none"> - LAI set to MODIS monthly means; - Revised minimum stomatal resistance for crops (from 180 to 100 sm^{-1}), short grass (from 110 to 100 sm^{-1}) and needle-leaf trees (from 500 to 250 sm^{-1}). 	<ul style="list-style-type: none"> Off-line runs driven by ERA-Interim (Jan 2009 – Dec 2010) with: - LAI set to MODIS monthly means; - Revised minimum stomatal resistance for crops (from 180 to 100 sm^{-1}), short grass (from 110 to 100 sm^{-1}) and needle-leaf trees (from 500 to 250 sm^{-1}). 	
MODIS LAI + Z_0	As cell above, but with revised Z_{oM} , Z_{oH} (see Table 2).	<ul style="list-style-type: none"> Off-line runs driven by ERA-Interim (Jan 2009 – Dec 2010) with: - As cell above, but with revised Z_{oM}, Z_{oH} 	
Skin Conductivity: MODIS LAI + Z_0 + Λ_{skin}	As cell above, but with Λ_{skin} original values (as indicated in Table 3) set to $\Lambda_{\text{skin}}/2$.	<ul style="list-style-type: none"> Off-line runs driven by ERA-Interim (Jan 2009 – Dec 2010) with: - As cell above, but with Λ_{skin} original values (as indicated in Table 3) set to $\Lambda_{\text{skin}}/2$. 	

Table 2. Roughness lengths for momentum and for heat.

Surface Type	Control		New Values	
	Z_{oM} (m)	Z_{oH} (m)	Z_{oM} (m)	Z_{oH} (m)
Bare soil	0.013	0.0013	0.013	0.00013
Crops, mixed farming	0.15	0.015	0.5	0.005
Short grass	0.02	0.002	0.2	0.002
Evergreen needle-leaf trees	2	2	2	2
Deciduous needle-leaf trees	2	2	2	2
Deciduous broad-leaf trees	2	2	2	2
Evergreen broad-leaf trees	2	2	2	2
Tall grass	0.1	0.01	0.47	0.0047
Desert	0.013	0.0013	0.013	0.0013
Tundra	0.05	0.005	0.034	0.00034
Irrigated crops	0.15	0.015	0.5	0.005
Semidesert	0.05	0.005	0.17	0.0017
Ice caps	0.0013	0.00013	0.0013	0.00013
Bogs and marshes	0.05	0.005	0.83	0.0083
Inland water	0.0001	0.00001	0.0001	0.00001
Ocean	0.0001	0.00001	0.0001	0.00001
Evergreen shrubs	0.1	0.01	0.37	0.0037
Deciduous shrubs	0.1	0.01	0.25	0.0025
Mixed forest	2	2	2	2
Interrupted forest	0.5	0.5	1.1	1.1

Table 3. Skin Conductivity, Λ_{skin} , values per surface tile. Unstable/stable refers to the temperature gradient between the skin layer and the top soil or snow layer.

Tile	$\Lambda_{\text{skin}} \text{ unstable (Wm}^{-2}\text{K}^{-1}\text{)}$	$\Lambda_{\text{skin}} \text{ stable (Wm}^{-2}\text{K}^{-1}\text{)}$
Bare Ground	15	15
Low Vegetation	10	10
High Vegetation	20	15
Snow on low vegetation/ bare ground	7	7
High Vegetation with snow beneath	20	15
Intercepted water	10	10
Ice water	58	58
Open water	∞	∞

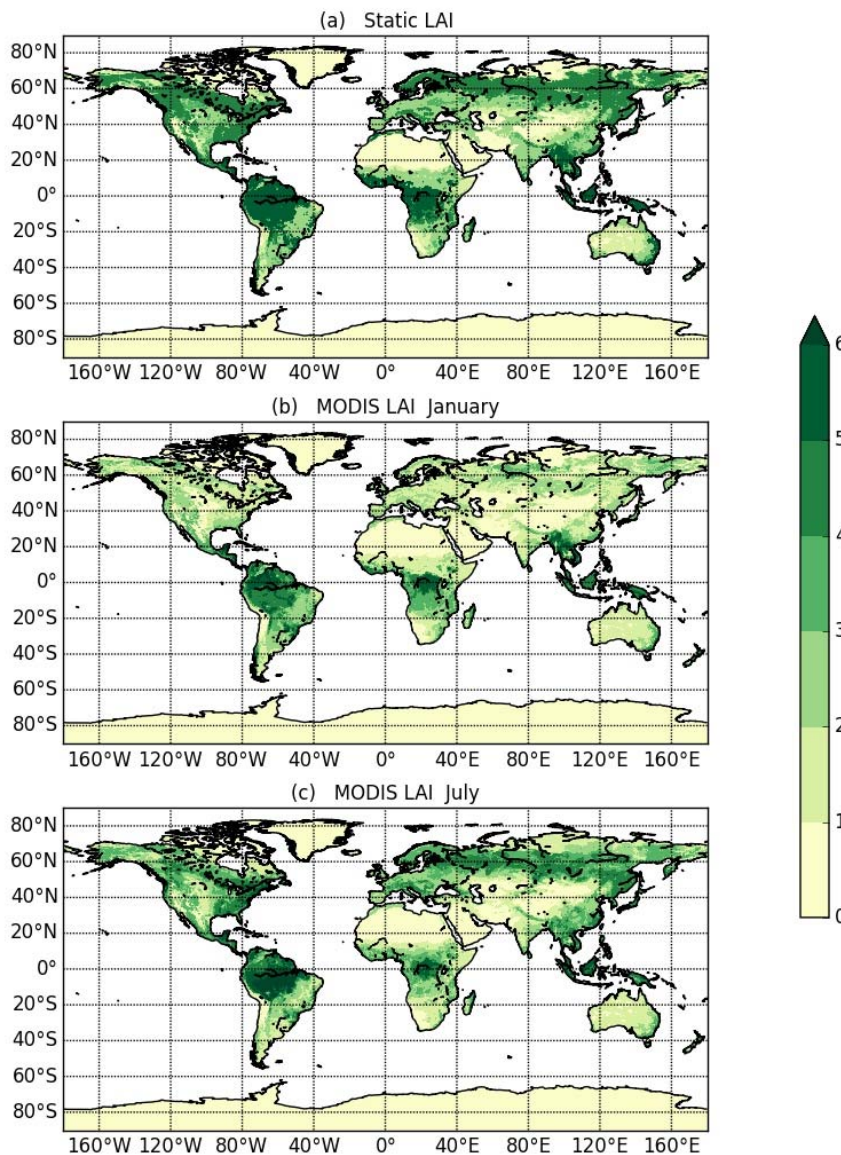


Figure 1 – (a) Total LAI (m^2/m^2) used in the control runs and as defined in the operational model until November 2010. MODIS monthly LAI climatology for (b) January and (c) July.

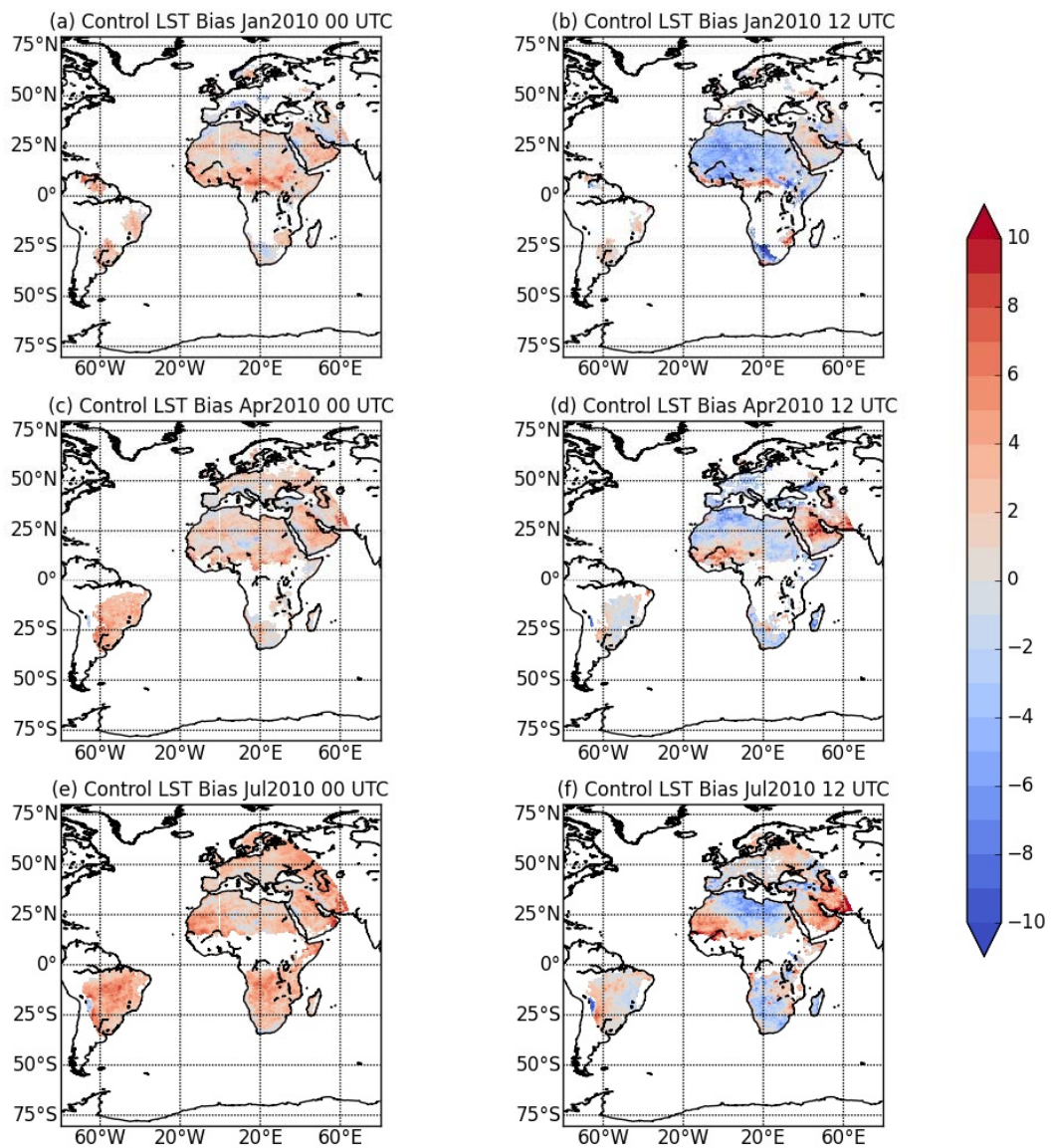


Figure 2- Skin temperature bias with respect to SEVIRI LST (ECMWF minus SEVIRI LST; °C) obtained for the control experiment for 0UTC (left) and 12 UTC (right panels), for January 2010 (top), April 2010 (middle) and July 2010 (bottom). Area coverage corresponds to the Meteosat disk (centred at 0° longitude), with a viewing zenith angle up to 70°.

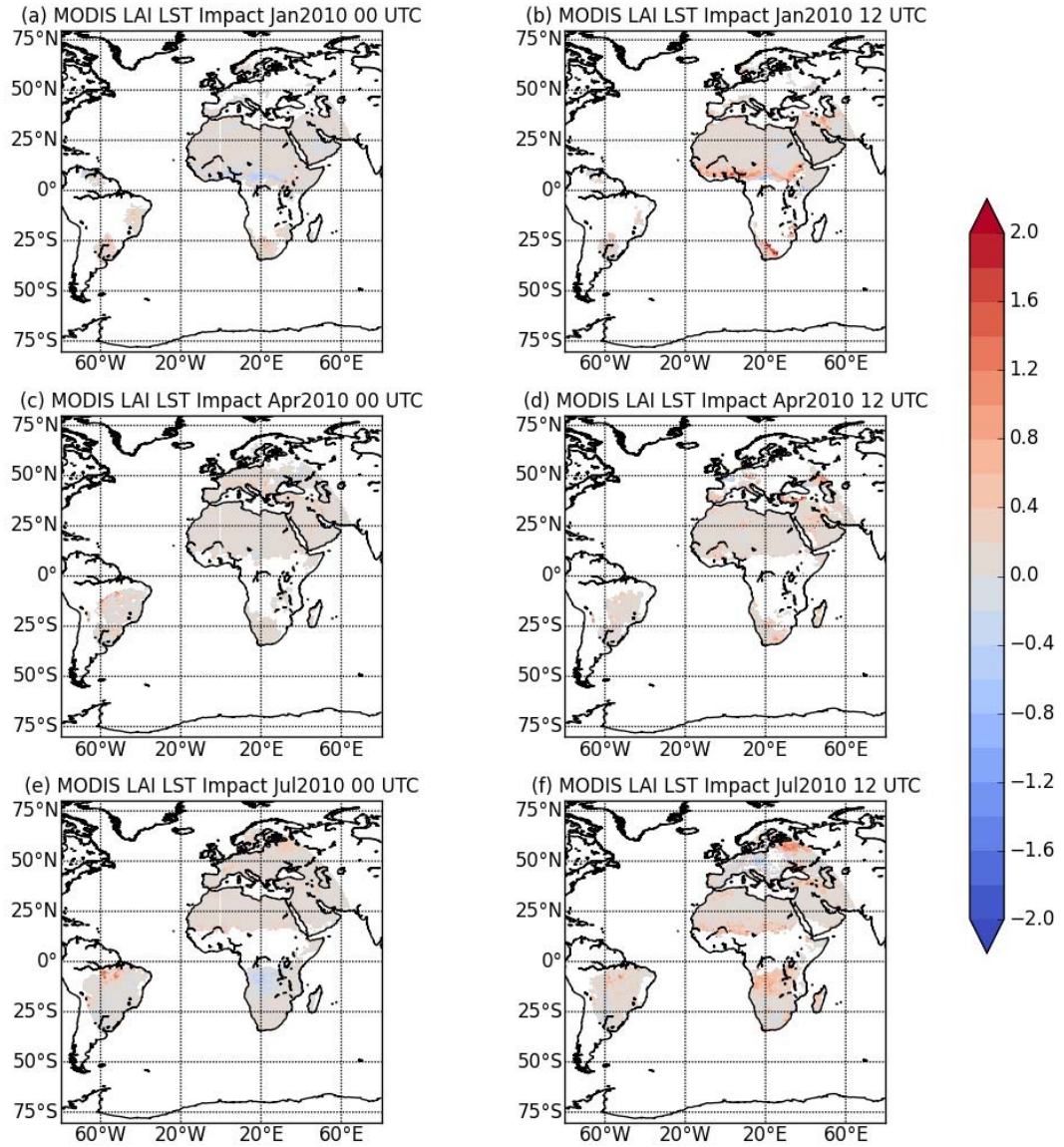


Figure 3 - Impact on model skin temperature ($^{\circ}\text{C}$), i.e., the difference in the mean absolute error (MAE) of the control minus the MAE of the forecast experiment with MODIS LAI, for 0UTC (left) and 12 UTC (right panels), for January 2010 (top), April 2010 (middle) and July 2010 (bottom).

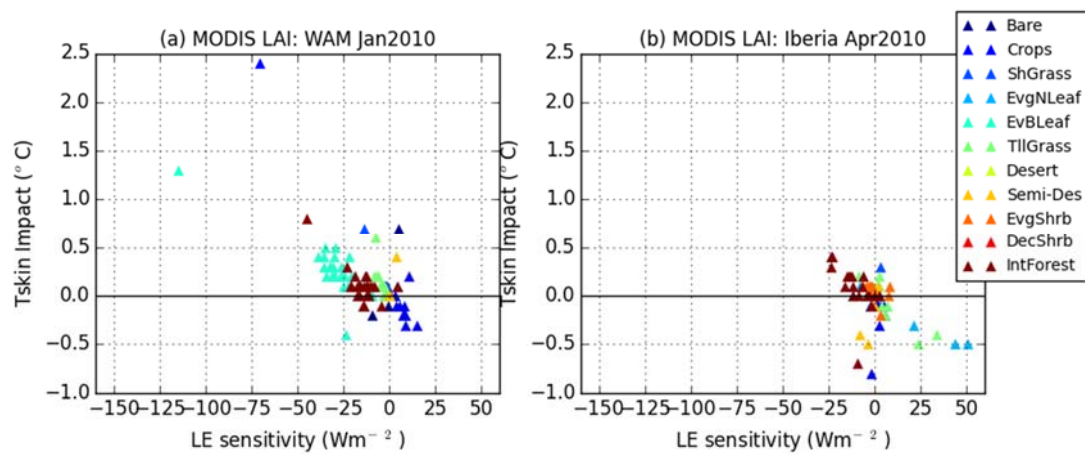


Figure 4 - Scatter plots of the difference in the mean absolute error of 12 UTC model skin temperature (impact in $^{\circ}\text{C}$) versus the difference of daily mean latent heat flux of MODIS LAI experiment minus the control (sensitivity in Wm^{-2}), for all model grid boxes within an area in the (a) West African monsoon (WAM) region [20°W – 10°E ; 2.5°N – 17.5°N] in January 2010; and (b) Iberian Peninsula [9.5°W – 0°E ; 36°N – 44°N] in April 2010. The dots are coloured according to the model land cover type.

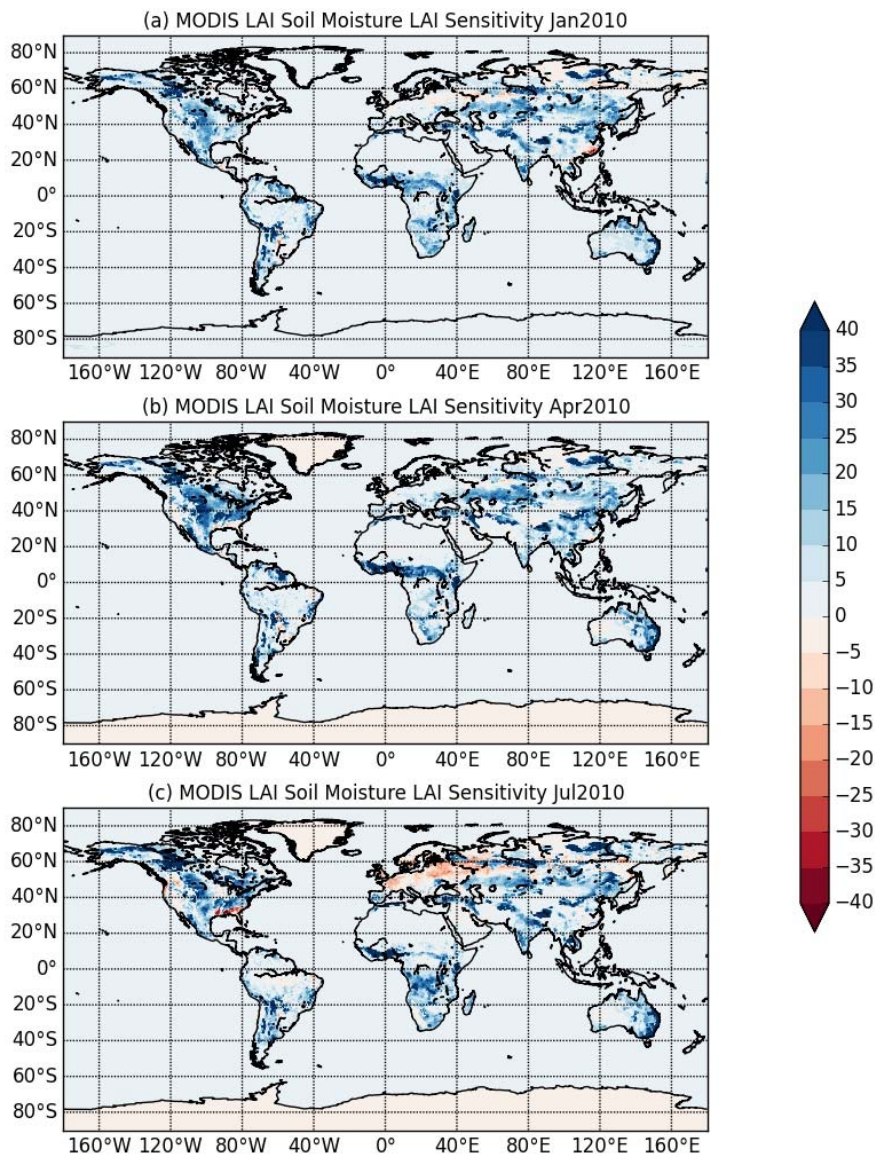


Figure 5 – Difference of daily Soil Moisture (mm) within the top 1m layer of soil: MODIS LAI experiment minus control. The panels represent averages over (a) January 2010; (b) April 2010; (c) July 2010.

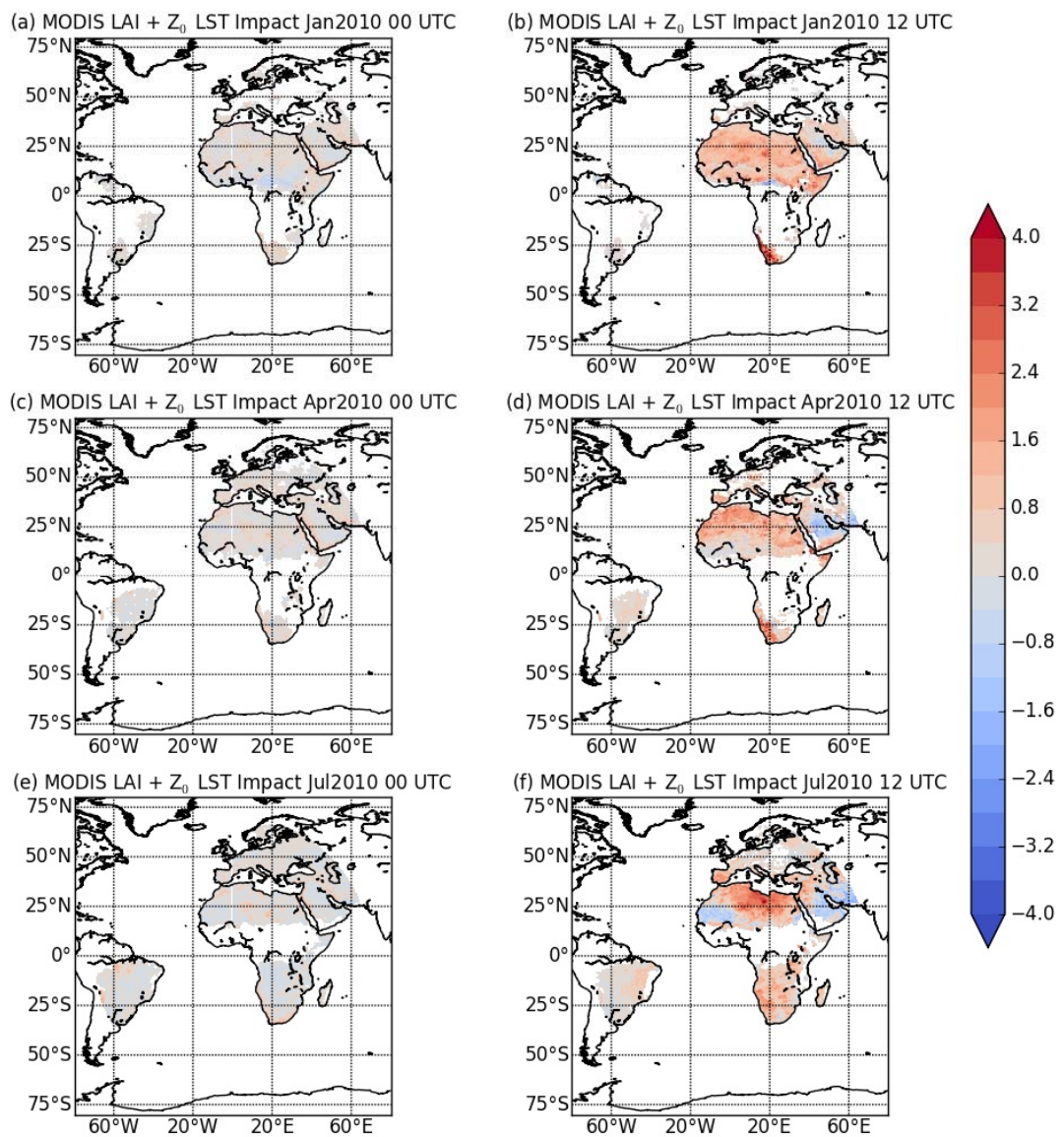


Figure 6 - As in Fig. 3, but for the experiment with MODIS LAI and revised roughness lengths for momentum and heat.

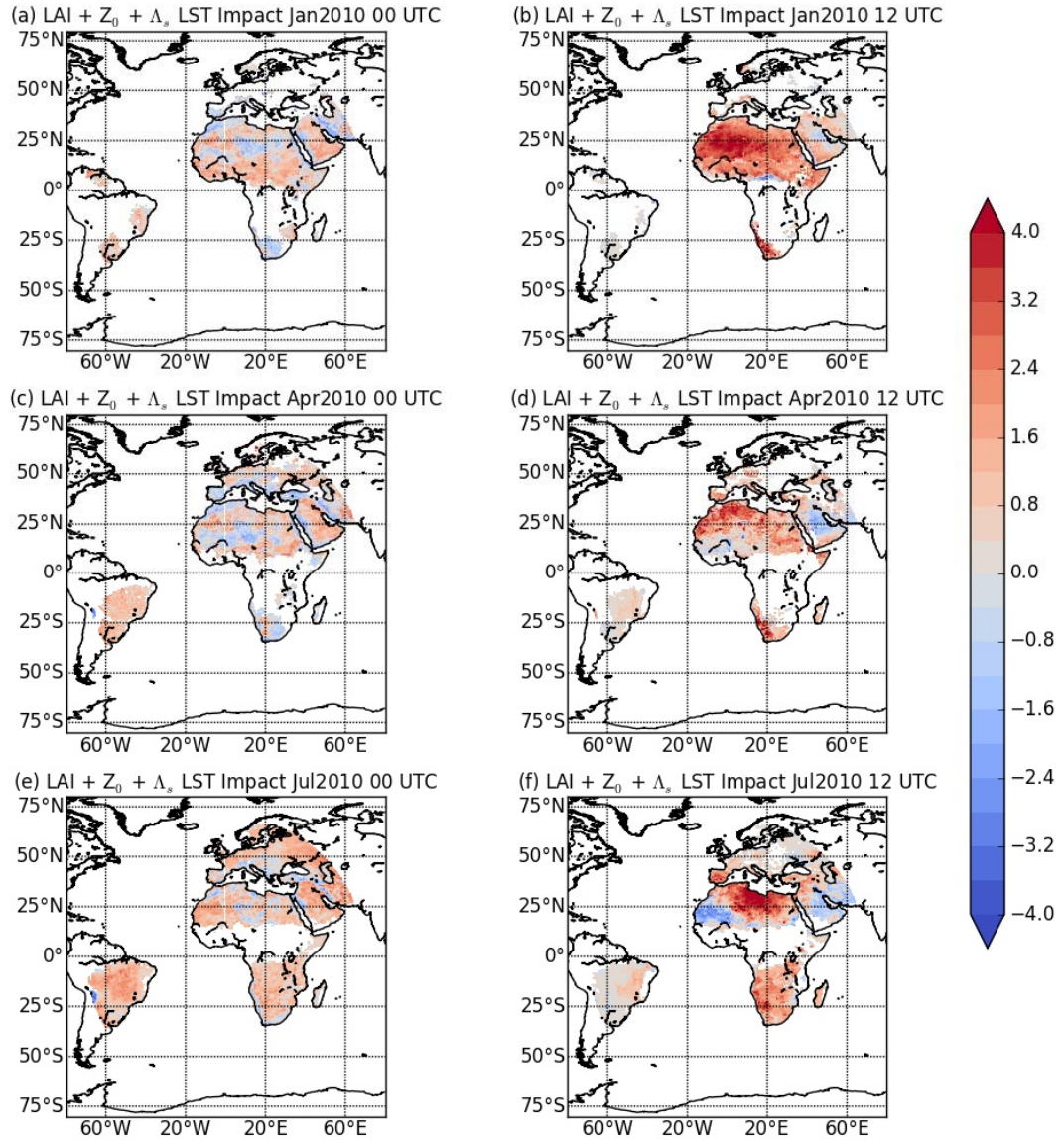


Figure 7 - As in Fig. 3, but for the experiment with MODIS LAI, revised roughness lengths for momentum and heat, and new skin conductivity table.

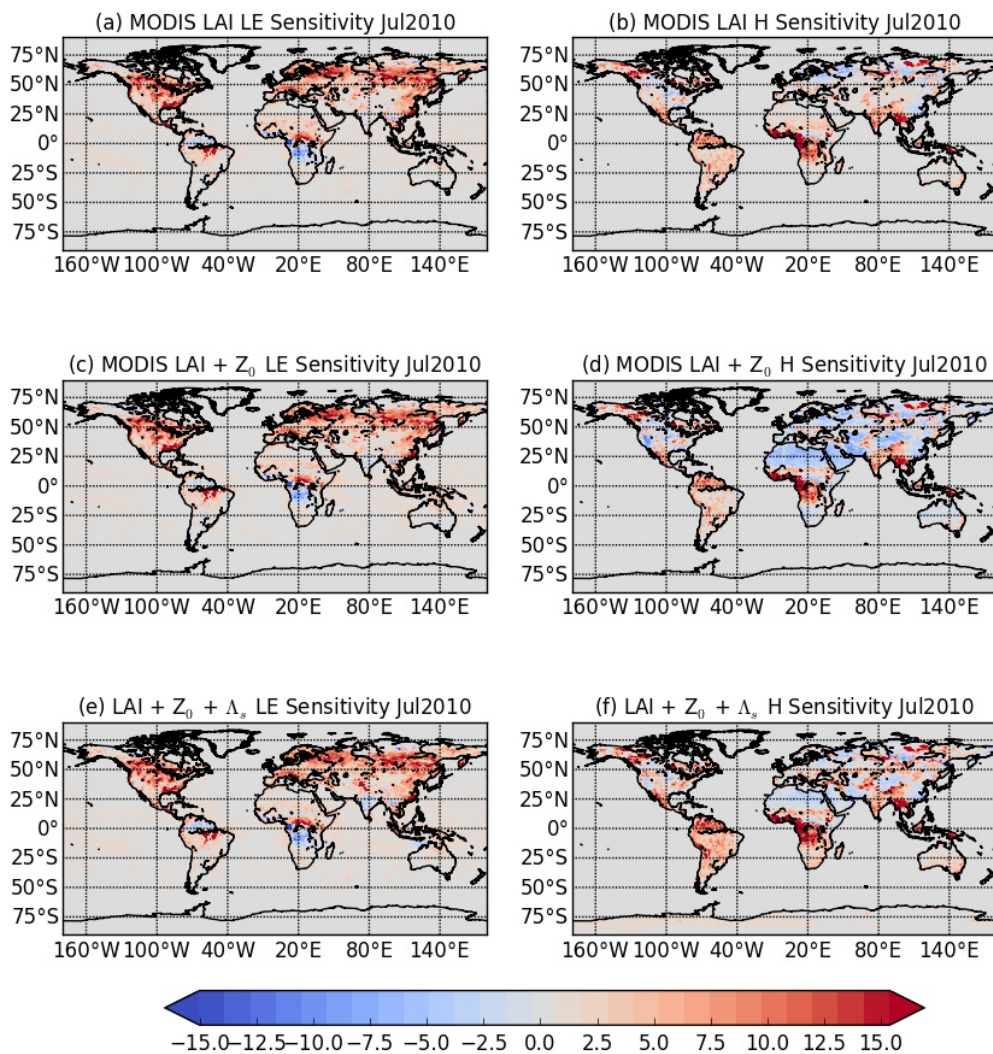


Figure 8 - Sensitivity of latent (LE in Wm^{-2} ; left panels) and sensible heat fluxes (H in Wm^{-2} ; right panels) averaged over July 2010, for (a) and (b) MODIS LAI; (c) and (d) MODIS LAI + Z₀; and (e) and (f) MODIS LAI + Z₀ + Λ_s experiments. Sensitivity is measured as the difference between each experiment and the control.

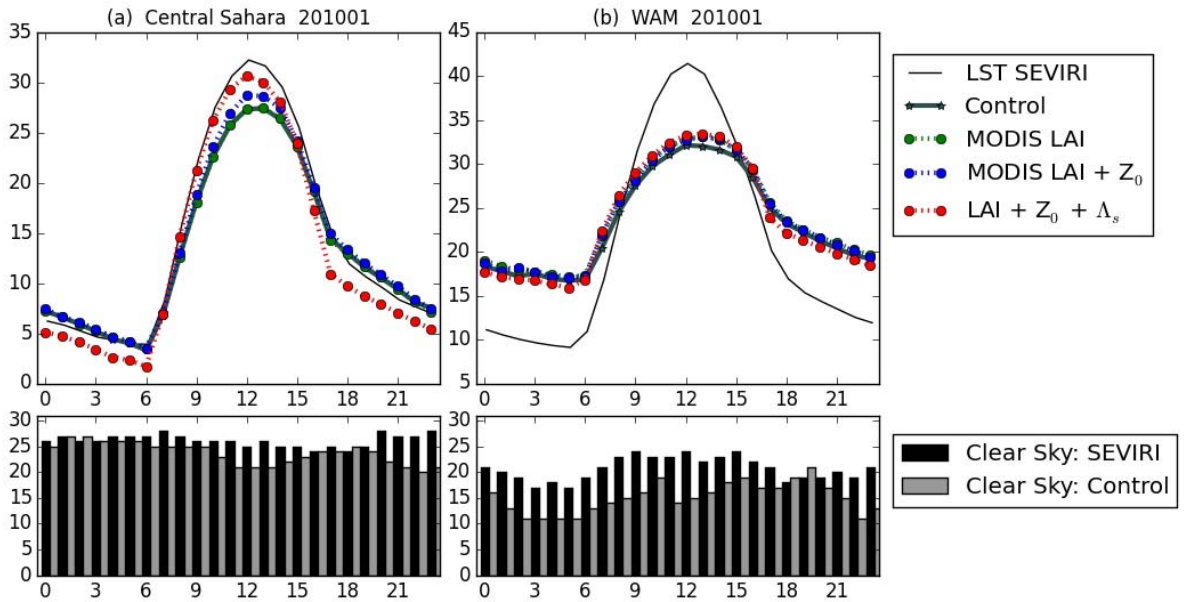


Figure 9 – Hourly LST ($^{\circ}$ C) and model Tskin ($^{\circ}$ C) averaged over January 2010 for grid points located in (a) Central Sahara (14.06° E; 26.37° N); and in (b) the West Africa Monsoon (WAM) region (13.71° E; 7.38° N). The black solid line corresponds to SEVIRI LST estimates and the remaining correspond to Tskin simulations (see figure legend). The lower panels indicate the number of clear sky cases per hour, which were taken into account to estimate the LST (black bars) and the control Tskin (grey bars) average daily cycle.